Available online at www.sciencedirect.com
ScienceDirect
Journal of Sound and Vibration 315 (2008) 239–257
JOURNAL OF SOUND AND VIBRATION
www.elsevier.com/locate/jsvi

Absorbent parallel noise barriers in urban environments

K.M. Li[a,*], M.K. Law[b], M.P. Kwok[b]

[a]*Ray W. Herrick Laboratories, School of Mechanical Engineering, The Purdue University, 140 Martin Jischke Drive, West Lafayette, IN 47907-2031, USA*
[b]*Department of Mechanical Engineering, The Hong Kong Polytechnic University, Hung Hom, Hong Kong*

Received 7 March 2007; received in revised form 31 January 2008; accepted 1 February 2008
Handling Editor: J. Lam
Available online 18 April 2008

Abstract

Theoretical and experimental studies are presented for the acoustic performance of parallel absorbent noise barriers in the presence of one or two parallel façade surfaces. A modified ray model has been developed to calculate the sound fields in these complex urban environments. The ray model has been validated by comparing with scale-model experiments and a wave-based computationally intensive numerical scheme. The barrier insertion loss is shown to be dependent on the source/receiver geometry, the acoustical property of the absorbent materials and the configuration of parallel noise barriers.
© 2008 Elsevier Ltd. All rights reserved.

1. Introduction

In a densely populated city with many high-rise buildings, noise pollution is one of the environmental problems that have been addressed with high priority. Dwellings, hospitals and other noise sensitive buildings are located in close proximity of major roadways. The transportation noise from an increasing traffic volume seriously deteriorates the quality of life of most citizens living in these densely populated cities. Among various measures for noise mitigation in high-rise cities, roadside noise barriers are one of the most extensively used methods for noise reduction. The noise barriers cut off the sight-line propagation of sound and hence reduce the noise levels at shadow regions. In many situations, parallel noise barriers are often built to achieve the required noise reductions. However, the huge construction cost and the esthetic aspects of noise barriers have stirred up public concerns on the merit of their installations. To evaluate the effectiveness of noise barriers, accurate predictions of the screening performance during the design stages are essential.

In the 1980s, Hutchins and Pitcarn [1] developed a laser technique to determine the acoustic wave paths generated from a source located between parallel barriers to the top of each barrier. Based on the theoretical model by Hurst [2] and assumption of incoherence nature of the source, they predicted the sound intensity levels at the top of barriers by summing the contributions from the principal wave propagation paths. Comparisons with upright and inclined parallel barriers were made also. Hutchins et al. [3,4] later presented

*Corresponding author.
E-mail address: mmkmli@purdue.edu (K.M. Li).

0022-460X/$ - see front matter © 2008 Elsevier Ltd. All rights reserved.
doi:10.1016/j.jsv.2008.02.023

scale-model investigations of the acoustic performance of parallel barriers with different geometrical configurations. Scale-model experiments have the advantage of permitting the control over many parameters in the experimental set-up that enables the assessment of the acoustic performance for a large range of barrier configurations to be made easily. Different barrier types were investigated and they found that a grass-covered slope surface appeared to be the most effective over the frequency range examined. They also concluded that the reflections from the inner face of the far-side parallel barrier were only significant when the source was close to this surface.

With the advent of modern computers, the models for barrier diffraction incorporated with ground effects have shifted from analytical models and experimental studies to computationally intensive numerical schemes, such as the boundary element formulation (BEM). Hothersall et al. [5–8] developed this type of numerical schemes for studying the shielding performance of different barriers over absorbing ground. Nevertheless, in a more recent study, Panneton et al. [9] used the image source method (ISM) to investigate the performance of parallel barriers. They extended the study to include absorption on inner barrier surfaces. Multiple reflections between the parallel barriers, diffraction solutions by Hadden and Pierce [10] and the modified Delany–Bazley impedance model by Miki [11] were used in their study. They presented experimental results to validate their theoretical models at the shadow region below the top edge of the barrier.

The current paper, which is an extension of our earlier studies [12,13], is motivated by the need to assess the combined effects of porous road pavements, absorbent surfaces of parallel barriers and building façades for maximizing the noise reductions for highways flanked by rows of tall buildings. We present the first step of this 'ultimate' model by studying the sound fields behind absorbent parallel noise barriers in the vicinity of tall buildings above a hard ground.

The paper is arranged as follows. Section 2 presents the formulation of the problem. A description of the ray model for parallel hard barriers is then reviewed. It is followed by presenting a modified ray model, which is used to calculate sound fields for absorbent parallel noise barriers placed in urban environments. The modified ray model is validated numerically in Section 3 by comparing with numerical predictions that is based on the boundary integral equations method. Section 4 presents the validation of the ray model by comparing with measured data obtained from indoor scale-model experiments. In Section 5, we present numerical simulations for a pair of absorbent parallel noise barriers placed above a hard ground in a street canyon. Numerical results suggest that the acoustic performance of the parallel barriers can be enhanced by placing sound absorptive materials on the surfaces facing each other. Concluding remarks are then offered in Section 6.

2. Theory

2.1. A ray model for parallel barriers of rigid surfaces

In an early study, Li et al. [13] developed a ray model for studying the sound field in the vicinity of parallel barriers in high-rise cities. First, they investigated the case of parallel barriers placed in front of a row of tall buildings. Secondly, they examined the case where the parallel barriers are placed in a street canyon. In the modeling process, all boundaries in the high-rise cities are perfectly reflecting surfaces. Nevertheless, both situations are identical except that an extra façade surface is placed parallel to the far-side barrier in the later case. For these two cases, they compared the theoretical and experimental results of the barrier insertion loss (IL) for different geometrical configurations. They demonstrated that their ray-based model provided accurate solutions that agreed reasonably well with indoor scaled-model experiments as well as with predictions according to the BEM formulation. Details of the ray model formulation will not be repeated but the major results are summarized here for the sake of completeness. See Fig. 1 for the schematic diagram of the problem and the symbols used in our subsequent formulation.

In Fig. 1, we show that the source and receiver are located in a street canyon with the presence of a pair of parallel barriers. The façade surface at the far side Γ_{F2} can be ignored if the problem for a pair of parallel barriers positioning in front of a façade is just considered. A close examination of the situation reveals that if a pair of barriers is aligned parallel to one or two rows of tall buildings, the sound field is composed of contributions from two main groups of rays. They are either the direct sight-line contributions from all

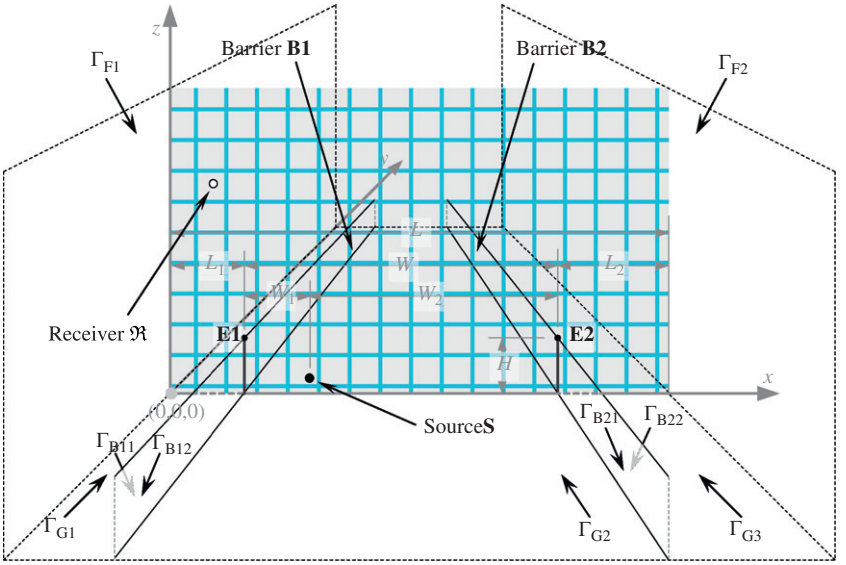

Fig. 1. Schematic diagram of the specified problem. A source **S** is located at (x_S, 0, z_S) and a receiver $\Re$ at (x_R, 0, z_R). A pair of parallel noise barriers, B1 and B2, of height H and their edges of **E1** and **E2**, are placed in a complex urban environment. This diagram shows the parallel noise barriers are placed inside a street canyon formed by two façade surfaces Γ_{F1} and Γ_{F2} of infinite height. The façade surface Γ_{F2} is absent in the case of a single building façade.

viewable image sources or the contributions of the sound diffracted at the barrier's top edge:

$$p(\mathbf{S},\Re) = P_{\text{direct}} + P_{\text{diffract}}. \tag{1}$$

In the illumination zone where $z_R > H$ and $x_R \leqslant L_1$, P_{direct} and P_{diffract} can be computed separately and the formulas are listed as follows:

(a) Parallel barriers in front of tall buildings:

$$P_{\text{direct}} = \sum_{m=m_<}^{m_>} G_d(\mathbf{S}_m, \Re_{\pm 1}) + \sum_{m=m_<}^{m_>} G_d(\mathbf{\Lambda}_m, \Re_{\pm 1}) \tag{2}$$

$$\begin{aligned} P_{\text{diffract}} = & \sum_{n=1}^{\infty} [G_f(\mathbf{S}_n, \Re_{\pm 1}|\mathbf{E}_1) + G_f(\mathbf{\Lambda}_n, \Re_{\pm 1}|\mathbf{E}_1)] \\ & + \sum_{n=1}^{\infty} [G_f(\mathbf{S}_n, \mathbf{\Psi}_{\pm 1}|\mathbf{E}_1) + G_f(\mathbf{\Lambda}_n, \mathbf{\Psi}_{\pm 1}|\mathbf{E}_1)] \\ & + \sum_{n=0}^{\infty} [G_f(\mathbf{S}_{-n}, \Re_{\pm 1}|\mathbf{E}_2) + G_f(\mathbf{\Lambda}_{-n}, \Re_{\pm 1}|\mathbf{E}_2)]. \end{aligned} \tag{3}$$

(b) Parallel barriers in a street canyon:

$$\begin{aligned} P_{\text{direct}} = & \sum_{j=0}^{\infty} \sum_{m=m_<(j)}^{m_>(j)} G_d(\mathbf{S}_m, \Re_{-j}) + \sum_{j=0}^{\infty} \sum_{m=m_<(j)}^{m_>(j)} G_d(\mathbf{\Lambda}_m, \Re_{-j}) \\ & + \sum_{j=1}^{\infty} \sum_{m=m_<(j)}^{m_>(j)} G_d(\mathbf{S}_{-m}, \Re_j) + \sum_{j=1}^{\infty} \sum_{m=m_<(j)}^{m_>(j)} G_d(\mathbf{\Lambda}_{-m}, \Re_j), \end{aligned} \tag{4}$$

$$P_{\text{diffract}} = \sum_{j=1}^{\infty}\sum_{n=1}^{\infty}[G_f(\mathbf{S}_n, \Re_{\pm j}|\mathbf{E}_1) + G_f(\mathbf{\Lambda}_n, \Re_{\pm j}|\mathbf{E}_1)] + \sum_{j=1}^{\infty}\sum_{n=1}^{\infty}[G_f(\mathbf{S}_n, \mathbf{\Psi}_{-j}|\mathbf{E}_1) + G_f(\mathbf{\Lambda}_n, \mathbf{\Psi}_{-j}|\mathbf{E}_1)] + \sum_{j=1}^{\infty}\sum_{n=0}^{\infty}[G_f(\mathbf{S}_n, \Re_{\pm j}|\mathbf{E}_2) + G_f(\mathbf{\Lambda}_c, \Re_{\pm j}|\mathbf{E}_2)]. \quad (5)$$

Here, P_{direct} includes all terms linking directly from the source and its images to the receiver and its corresponding images. If the receiver is located at the shadow zone where $z_R \leqslant H$ and $x_R \leqslant L_1$, then the sound field is the same for (a) and (b). There is no contribution from the direct fields but the total diffracted sound field is given by

$$P_{\text{diffract}} = \sum_{n=1}^{\infty}\sum_{j=0}^{\infty}[G_f(\mathbf{S}_n, \Re_{-j}|\mathbf{E}_1) + G_f(\mathbf{\Lambda}_n, \Re_{-j}|\mathbf{E}_1)] + \sum_{n=1}^{\infty}\sum_{j=0}^{\infty}[G_f(\mathbf{S}_n, \mathbf{\Psi}_{-j}|\mathbf{E}_1) + G_f(\mathbf{\Lambda}_n, \mathbf{\Psi}_{-j}|\mathbf{E}_1)]. \quad (6)$$

In Eqs. (2)–(6) $(\ldots,\mathbf{S}_{-2}, \mathbf{S}_{-1}, \mathbf{S}_0)\in\mathbf{S}_-$ and $(\mathbf{S}_1, \mathbf{S}_2, \mathbf{S}_3, \ldots)\in\mathbf{S}_+$ are the image sources formed because of the multiple reflections between the inner surfaces of the parallel barriers. The image sources, $(\ldots,\mathbf{\Lambda}_{-2},\mathbf{\Lambda}_{-1},\mathbf{\Lambda}_0)\in\mathbf{\Lambda}_-$ and $(\mathbf{\Lambda}_1,\mathbf{\Lambda}_2,\mathbf{\Lambda}_3, \ldots)\in\mathbf{\Lambda}_+$, are the respective images of $\mathbf{S}_-$ and $\mathbf{S}_+$ because of the reflection of the ground surface. The image sources, $\mathbf{S}_-$ and $\mathbf{\Lambda}_-$, are situated at the left of the far-side barrier, B2. The other two sets, $\mathbf{S}_+$ and $\mathbf{\Lambda}_+$, are positioned at the right of the near-side barrier, B1. The edges of near- and far-side barriers are denoted by **E1** and **E2**, respectively.

Similarly, four rows of image receivers can be formed because of the reflections of the parallel surfaces and the ground. The image receivers $(\ldots, \Re_{-2}, \Re_{-1}, \Re_0)\in\Re_-$ and $(\Re_1, \Re_2, \Re_3, \ldots)\in\Re_+$, are located above the ground while $(\ldots, \mathbf{\Psi}_{-2}, \mathbf{\Psi}_{-1}, \mathbf{\Psi}_0)\in\mathbf{\Psi}_-$ and $(\mathbf{\Psi}_1, \mathbf{\Psi}_2, \mathbf{\Psi}_3, \ldots)\in\mathbf{\Psi}_+$ are sited below the ground. Note that $\mathbf{S}_0(\equiv\mathbf{S}_1)$ and $\Re_0(\equiv\Re_1)$ are the source and receiver, respectively. The symbols, $\mathbf{\Lambda}_0(\equiv\mathbf{\Lambda}_1)$ and $\mathbf{\Psi}_0(\equiv\mathbf{\Psi}_1)$, are the ground reflected terms of the source and receiver, respectively. Their introductions lead to a more compact form of the ray series for representing the sound fields.

It is noted in Eqs. (2) and (4) that the ray series for the image sources $\mathbf{S}_m$ is limited to the range from $m_<$ to $m_>$. They correspond to the image sources that can set up sight-line contacts with the respective image receivers. These limits are dependent on the geometrical configuration of the problem.

By identifying these image sources and image receivers, we can write the direct and diffracted field as a sum of different series of rays. In Eqs. (2)–(6), the general form of the Green function $G_d(\mathbf{S}, \mathbf{R})$ is the free field sound pressure emanating from a source point at $\mathbf{S}$ to an arbitrary field point at $\mathbf{R}$. On the other hand, $G_f(\mathbf{S}, \mathbf{R}|\mathbf{E}_1)$ is the corresponding Green function for the diffracted sound pressure at a field point $\mathbf{R}$ from a source point at $\mathbf{S}$ due to the edge $\mathbf{E}$ of a rigid barrier where $(\mathbf{E_1}, \mathbf{E_2})\in\mathbf{E}$.

2.2. A modified ray model for absorptive boundary surfaces

Rigid boundaries are considered earlier in the analysis for parallel noise barriers in the high-rise cites. In these cases, the spherical wave reflection coefficient for each interaction of sound waves with a plane boundary is simply equal to 1, i.e., an incoming wave have the same magnitude and phase as their reflected waves. However, the idea can be readily extended to include any boundaries with finite impedance.

Here, we present the case of sound field due to a point source near a locally reacting surface. The spherical wave reflection coefficient, Q can be computed according to Ref. [14] as follows:

$$Q(\mathbf{S}, \mathbf{R}, \beta) = R_p + (1 - R_p)F(w), \quad (7)$$

where R_p is the plane wave reflection coefficient given by

$$R_p = \frac{\cos\theta - \beta}{\cos\theta + \beta}, \tag{8}$$

where θ is the incident angle of the reflected wave of for a source and receiver located at **S** and **R**, respectively. The angle of incident can be determined straightforwardly for a given source/receiver geometry. The term $F(w)$ in Eq. (7) is also known as the boundary loss factor, which is given by

$$F(w) = 1 + \mathrm{i}\sqrt{\pi} w \mathrm{e}^{-w^2}\,\mathrm{erfc}(-\mathrm{i}w), \tag{9}$$

where erfc is the complimentary error function and the numerical distance, w, is defined by

$$w = \tfrac{1}{2}\sqrt{kd}(1+\mathrm{i})(\cos\theta + \beta) \tag{10}$$

with k the wavenumber of the source and d the distance from **S** to **R**. We also note that the spherical wave reflection coefficient can be modified accordingly for each interaction with a plane boundary [15].

Note that the contribution of the second term in Eq. (7) acts as a correction term because the wavefront is spherical rather than planar. The term $F(w)$ describes the interaction of a curved wavefront with a plane surface of finite impedance. If the source is located at a long distance from the plane of reflection (i.e., higher order of geometrical images), the wavefront becomes plane, and the reflection is non-grazing, then $|w| \to \infty$ and $F(w) \to 0$. If the surface is acoustically hard, then $|\beta| \to 0$ which implies $|w| \to 0$ and $F(w) \to 1$. Consequently, the spherical wave reflection coefficients, Q, for higher order image sources can be approximated by their respective plane wave reflection coefficients, R_p. These images may be treated effectively as point sources with a modified directivity.

Suppose now the boundary surfaces of our problem have finite impedances absorbing sound energies radiated from a noise source. Each of these surfaces is characterized acoustically with a specific normalized admittance. They are given, respectively, as β_{F1}, β_{F2}, β_{B11}, β_{B12} β_{B21}, β_{B22}, β_{G1}, β_{G2} and β_{G3} for the left façade surface Γ_{F1}, the right façade surface Γ_{F2}, the outer and inner surfaces of the near-side barrier Γ_{B1}, the inner and outer surfaces of the far-side barrier Γ_{B2}, the ground Γ_{G1} (which is the ground surface between the Γ_{F1} and Γ_{B1}), the ground Γ_{G2} (which is the ground surface between both barriers), and the ground Γ_{G3} (which is the ground surface behind the far-side barrier). The various notations of the admittance are shown in Fig. 1. We denote the respective spherical wave reflection coefficients as Q_{F1}, Q_{F2}, Q_{B11}, Q_{B12} Q_{B21}, Q_{B22}, Q_{G1}, Q_{G2} and Q_{G3} for the calculation of sound reflected from these surfaces.

We also need to modify the Green function for the sound diffracted by an absorptive barrier. For a given source **S**, receiver **R** and the barrier with the wedge's edge at **E**, the diffraction T can be computed by adopting the Koers [16] modification of the Hadden and Pierce [10] solution to an absorbing wedge. Using the notation shown in Fig. 2, T is given as follows:

$$T(S,R,|E,\beta_S,\beta_R) = U_1 + Q_S U_2 + Q_R U_3 + Q_S Q_R U_4, \tag{11}$$

where β_S and β_R are the respective specific normalized admittance of barrier's surfaces facing the source and receiver. The function, $Q_S = Q\ (S,\ E,\ \beta_S)$ and $Q_R = Q\ (E,\ R,\ \beta_R)$ are the corresponding spherical wave reflection coefficients at the sides facing the source and receiver. Both Q_S and Q_R can be computed by using

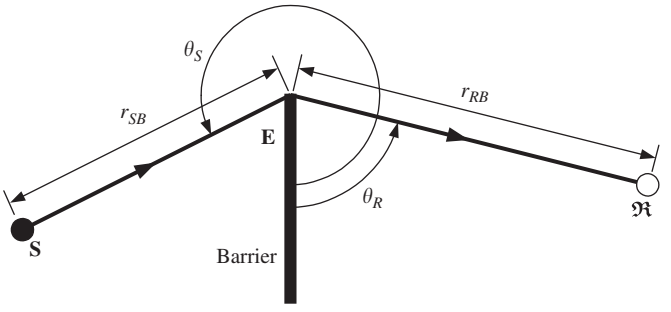

Fig. 2. Schematic diagram showing the diffraction of sound by a thin absorbent noise barrier.

Eq. (7). In Eq. (11), the function U_i (for $i = 1$, 2, 3 and 4) is given by

$$U_i \equiv U(\vartheta_i, r_{SB}, r_{RB}) = -\frac{1}{\pi} A(\vartheta_i)\left(\frac{\mathrm{e}^{\mathrm{i}kD}}{D}\right)\int_0^\infty \mathrm{e}^{-\zeta} G(\zeta, \vartheta_i, r_{SB}, r_{RB})\,\mathrm{d}\zeta, \tag{12}$$

where r_{SB} and r_{RB} are the respective distances measured from **S** to **E** and from **E** to **R**. The parameter, ζ, is a dummy variable for the integral and ϑ_i is the relative angle defined by

$$\vartheta_i = \begin{cases} |\theta_R - \theta_S| & \text{for } i = 1, \\ 2\pi - \theta_S - \theta_R & \text{for } i = 2, \\ \theta_S + \theta_R & \text{for } i = 3, \\ 2\pi - |\theta_R - \theta_S| & \text{for } i = 4. \end{cases} \tag{13}$$

Here, θ_s and θ_r are the respective angular positions of **S** and **R** measured from the polar plane at the side of the barrier surface facing the source. In Eq. (12), the function $A(\vartheta_i)$ and $G(\zeta, \vartheta_i, r_{SB}, r_{RB})$ are defined, respectively, as follows:

$$A(\vartheta_i) = \begin{cases} (\pi - \vartheta_i)/4 & \text{if } \pi \geqslant \vartheta_i, \\ -(3\pi + \vartheta_i)/4 & \text{if } \pi < \vartheta_i, \end{cases} \tag{14}$$

$$G(\zeta, \vartheta_i, r_{SB}, r_{RB}) = \frac{1}{A(\vartheta_i)}\left(1 + \frac{\mathrm{i}}{kD + \mathrm{i}\zeta}\right)\left(\frac{kD}{kD + \mathrm{i}\zeta}\right) \times \tan^{-1}\left[\tan[A(\zeta_i)]\tanh\left\{\sinh^{-1}\left[\frac{\zeta D}{kr_{SB}r_{RB}}\left(\frac{\mathrm{i}}{2} - \frac{\zeta}{4kD}\right)\right]\Big/2\right\}\right], \tag{15}$$

where D is the total length measured from the source to receiver via the wedge's edge, i.e.

$$D = r_{SB} + r_{RB}. \tag{16}$$

The integral of Eq. (12) for each term U_i can be evaluated numerically by use of the standard Laguerre technique [17].

We can now integrate the effect of multiple reflections from finite impedance surfaces into the ray model described earlier in Eqs. (7)–(16). In the illumination zone where $z_R > H$ and $x_R \leqslant L_1$, P_{direct} and P_{diffract} are given as follows:

(a) Parallel barriers in front of tall buildings:

$$p_{\text{direct}} = \sum_{j=0}^{1}\sum_{m_<(j)}^{m_>(j)} \Delta_{b2}(m)\Delta_{fb}(j)G_d(\mathbf{S}_m, \mathbf{R}_{-j}) + \sum_{j=0}^{1}\sum_{m_<(j)}^{m_>(j)} \Delta_{b2}(m)\Delta_{fb}(j)Q_{G2}G_d(\mathbf{\Lambda}_m, \mathbf{R}_{-j}), \tag{17}$$

$$\begin{aligned} p_{\text{diffract}} = {} & \sum_{j=0}^{1}\sum_{n=1}^{\infty} \Delta_{b2}(n)\Delta_{fb}(j)T(\mathbf{S}_n, \mathbf{R}_{-j}|\mathbf{E}_1, \beta_{12}, \beta_{11}) \\ & + \sum_{j=0}^{1}\sum_{m=1}^{\infty} \Delta_{b2}(n)\Delta_{fb}(j)Q_{G1}T(\mathbf{S}_n, \mathbf{\Psi}_{-j}|\mathbf{E}_1, \beta_{12}, \beta_{11}) \\ & + \sum_{j=0}^{1}\sum_{n=1}^{\infty} \Delta_{b2}(n)\Delta_{fb}(j)Q_{G2}T(\mathbf{\Lambda}_n, \mathbf{R}_{-j}|\mathbf{E}_1, \beta_{12}, \beta_{11}) \\ & + \sum_{j=0}^{1}\sum_{n=1}^{\infty} \Delta_{b2}(n)\Delta_{fb}(j)Q_{G1}Q_{G2}T(\mathbf{\Lambda}_n, \mathbf{\Psi}_{-j}|\mathbf{E}_1, \beta_{12}, \beta_{11}) \end{aligned}$$

$$+\sum_{j=0}^{1}\sum_{n=0}^{\infty}\Delta_{b1}(n)\Delta_{fb}(j)T(\mathbf{S}_{-n},\mathbf{R}_{-j}|\mathbf{E}_2,\beta_{21},\beta_{22})$$

$$+\sum_{j=0}^{1}\sum_{n=0}^{\infty}\Delta_{b1}(n)\Delta_{fb}(j)Q_{G2}T(\mathbf{\Lambda}_{-n},\mathbf{R}_{-j}|\mathbf{E}_2,\beta_{21},\beta_{22}), \tag{18}$$

where $\Delta_{b1}(M)$ ($M=m$ or n) is the reflection factor because there are M reflections from the inner surfaces of the both barriers for $\mathbf{S}_M$ and $\mathbf{\Lambda}_M$. The reflection factor $\Delta_{b2}(M)$ is that for $\mathbf{S}_{-M}$ and $\mathbf{\Lambda}_{-M}$ where there are $M-1$ reflections from the barriers' inner surfaces. Similarly, $\Delta_{fb}(j)$ is the reflection factor as there are j reflections from the left façade surface and the outer surface of the near-side barrier for the image receiver $\mathbf{R}_{-j}$. In general, these reflection factors can be determined for an integral value M by counting the number of reflections from each of these boundary surfaces and multiplying their respective spherical wave reflection coefficients. There are two general forms for these reflection factors as follows:

$$\Delta_R(Q_L,Q_R,M)=\begin{cases}(Q_LQ_R)^{(M-1)/2} & \text{when } M \text{ is odd},\\ Q_R(Q_LG_R)^{(M/2)-1} & \text{when } M \text{ is even}\end{cases} \tag{19}$$

and

$$\Delta_L(M)=\begin{cases}Q_L(Q_LQ_R)^{(M-1)/2} & \text{when } M \text{ is odd},\\ (Q_LG_R)^{M/2} & \text{when } M \text{ is even},\end{cases} \tag{20}$$

where Q_L and Q_R are the respective spherical wave reflection coefficients for the inner surfaces of the left and right side of the parallel boundaries. The parameter M is a positive integral value that represents the order of reflections. It can then be identified immediate that $\Delta_{b1}(M)\equiv\Delta_L(Q_{B12},Q_{B21},M)$, $\Delta_{b2}(M)\equiv\Delta_R(Q_{B12},Q_{B21},M)$ and $\Delta_{fb}(j)\equiv\Delta_L(Q_{F1},Q_{B11},j)$.

(b) Parallel barriers in a street canyon:

$$p_{\text{direct}}=\sum_{j=1}^{\infty}\sum_{m_<(j)}^{m_>(j)}\Delta_{b2}(m)\Delta_{f1}(j)G_d(\mathbf{S}_m,\mathbf{R}_{-j})+\sum_{j=1}^{\infty}\sum_{m_<(j)}^{m_>(j)}\Delta_{b2}(m)\Delta_{f2}(j)Q_{G2}G_d(\mathbf{\Lambda}_m,\mathbf{R}_{-j})$$
$$+\sum_{j=1}^{\infty}\sum_{m_<(j)}^{m_>(j)}\Delta_{b1}(m)\Delta_{f2}(j)G_d(\mathbf{S}_{-m},\mathbf{R}_j)+\sum_{j=1}^{\infty}\sum_{m_<(j)}^{m_>(j)}\Delta_{b1}(m)\Delta_{f2}(j)Q_{G2}G_d(\mathbf{\Lambda}_{-m},\mathbf{R}_j), \tag{21}$$

$$p_{\text{diffract}}=\sum_{j=1}^{\infty}\sum_{n=1}^{\infty}\Delta_{b2}(n)[\Delta_{f1}(j)T(\mathbf{S}_n,\mathbf{R}_{-j}|\mathbf{E}_1,\beta_{12},\beta_{11})+\Delta_{f2}(j)T(\mathbf{S}_n,\mathbf{R}_j|\mathbf{E}_1,\beta_{12},\beta_{11})]$$
$$+\sum_{j=1}^{\infty}\sum_{n=1}^{\infty}\Delta_{b2}(n)Q_{G2}[\Delta_{f1}(j)T(\mathbf{\Lambda}_n,\mathbf{R}_{-j}|\mathbf{E}_1,\beta_{12},\beta_{11})+\Delta_{f2}(j)T(\mathbf{\Lambda}_n,\mathbf{R}_j|\mathbf{E}_1,\beta_{12},\beta_{11})]$$
$$+\sum_{j=1}^{\infty}\sum_{n=1}^{\infty}\Delta_{b2}(n)\Delta_{f2}(j)Q_{G1}T(\mathbf{S}_n,\mathbf{\Psi}_{-j}|\mathbf{E}_1,\beta_{12},\beta_{11}),$$
$$+\sum_{j=1}^{\infty}\sum_{n=1}^{\infty}\Delta_{b2}(n)\Delta_{f2}(j)Q_{G1}Q_{G1}T(\mathbf{\Lambda}_n,\mathbf{\Psi}_{-j}|\mathbf{E}_1,\beta_{12},\beta_{11})$$
$$+\sum_{j=1}^{\infty}\sum_{n=0}^{\infty}\Delta_{b1}(n)[\Delta_{f1}(j)T(\mathbf{S}_{-n},\mathbf{R}_{-j}|\mathbf{E}_2,\beta_{21},\beta_{22})+\Delta_{f2}(j)T(\mathbf{S}_{-n},\mathbf{R}_j|\mathbf{E}_2,\beta_{21},\beta_{22})]$$
$$+\sum_{j=1}^{\infty}\sum_{n=0}^{\infty}\Delta_{b1}(n)Q_{G2}[\Delta_{f1}(j)T(\mathbf{\Lambda}_{-n},\mathbf{R}_{-j}|\mathbf{E}_2,\beta_{21},\beta_{22})+\Delta_{f2}(j)T(\mathbf{S}_{-n},\mathbf{R}_j|\mathbf{E}_2,\beta_{21},\beta_{22})], \tag{22}$$

where $\Delta_{f1}(j) \equiv \Delta_L(Q_{F1}, Q_{F2}, j)$ and $\Delta_{f2}(j) \equiv \Delta_R(Q_{F1}, Q_{F2}, j)$ are the respective reflection factors for the multiple reflections of the ray at the parallel façade surfaces before it reaches the image receivers. Finally, the sound field in the shadow zone in the region, $z_R \leqslant H$ and $x_R \leqslant L_1$ is composed of diffracted terms only as all the direct ray paths have been blocked by the near-side barrier. The diffracted field is given by

$$\begin{aligned} p_{\text{diffract}} = & \sum_{j=0}^{\infty}\sum_{n=1}^{\infty} \Delta_{b2}(n)\Delta_{fb}(j) T(\mathbf{S}_n, \mathbf{R}_{-j}|\mathbf{E}_1, \beta_{12}, \beta_{11}) \\ & + \sum_{j=0}^{\infty}\sum_{n=1}^{\infty} \Delta_{b2}(n)\Delta_{fb}(j) Q_{G1} T(\mathbf{S}_n, \mathbf{\Psi}_{-j}|\mathbf{E}_1, \beta_{12}, \beta_{11}) \\ & + \sum_{j=0}^{\infty}\sum_{n=1}^{\infty} \Delta_{b2}(n)\Delta_{fb}(j) Q_{G2} T(\mathbf{\Lambda}_n, \mathbf{R}_{-j}|\mathbf{E}_1, \beta_{12}, \beta_{11}) \\ & + \sum_{j=0}^{\infty}\sum_{n=1}^{\infty} \Delta_{b2}(n)\Delta_{fb}(j) Q_{G1} Q_{G2} T(\mathbf{\Lambda}_n, \mathbf{\Psi}_{-j}|\mathbf{E}_1, \beta_{12}, \beta_{11}). \end{aligned} \tag{23}$$

Owing to the fact that contributions from multiple diffractions are negligibly small, the sound fields in this region are the same for cases (a) and (b) described above because there will be no contributions from the edge of the far-side barrier. We remark that each of the terms in the equation listed above consists of a composite reflection factor, which accounts for the interaction of a contributory ray with the boundary surfaces. The respective spherical wave reflection coefficient is multiplied for every time a ray hits a boundary surface. The total sound field is obtained by summing the contributions from all possible rays linking the source with the receiver.

3. Numerical comparisons with the BEM

The ray model given in the last section has been implemented to compute the sound fields of typical urban environments with parallel barriers for shielding traffic noise sources. For validation, the computed results are compared with a wave-based BEM, which is based on the classical Helmholz integral equation. It is a powerful numerical tool, which has been widely used to study the propagation of sound outdoors. The BEM formulation is frequently used to study the acoustic performance of a noise barrier. However, the BEM calculation is computationally intensive especially for the case at high frequencies with large source/receiver separation in a complex urban environment. This drawback encourages the development of a ray model to predict the sound fields in these situations.

A typical outdoor configuration is used in our numerical analysis, see Fig. 3. In all cases, the near- and far-side barriers, B1 and B2, have an identical height of 2.5 m, and are situated at 5 and 15 m in front of the building façade, F1. An omni-directional noise source is located at 0.25 m above the ground and 7.5 m in front of the near-side barrier. As can be seen in Fig. 3, cases (I) and (II) represent the case of parallel barriers in front of the building façades. For cases (III) and (IV), an extra façade surface F2 is located at 5 m away from the barrier B2. In order words, this additional façade is located at 20 m from F1. It represents the case of a pair of parallel barriers erected in a street canyon. In our numerical simulations, the receivers are chosen at 1 m away from the façade F1 at various heights. The choice of these source/receiver geometries allows our numerical models to examine the sound fields in different areas of interest—the shadow, penumbra and illumination zones.

For the case of a pair of absorbent barriers placed in front of a row of tall buildings, the receiver is placed at illumination zone at (1, 0, 10) for case (I). It is placed at the shadow zone at (1, 0, 1) m in case (II). For the case of street canyon, we choose the receiver to be located at (1, 0, 5) m in the penumbra region for case (III) and at (1, 0, 2) m in the shadow zone for case (IV). The sound fields for other source/receiver geometries have also been computed but, for brevity, we only present typical results for these four cases. To assess the effectiveness of the absorbent parallel barriers, only the inner surface of both barriers is assumed to be absorptive. All other surfaces, including the building façade and ground, are assumed to be perfectly reflecting boundaries because

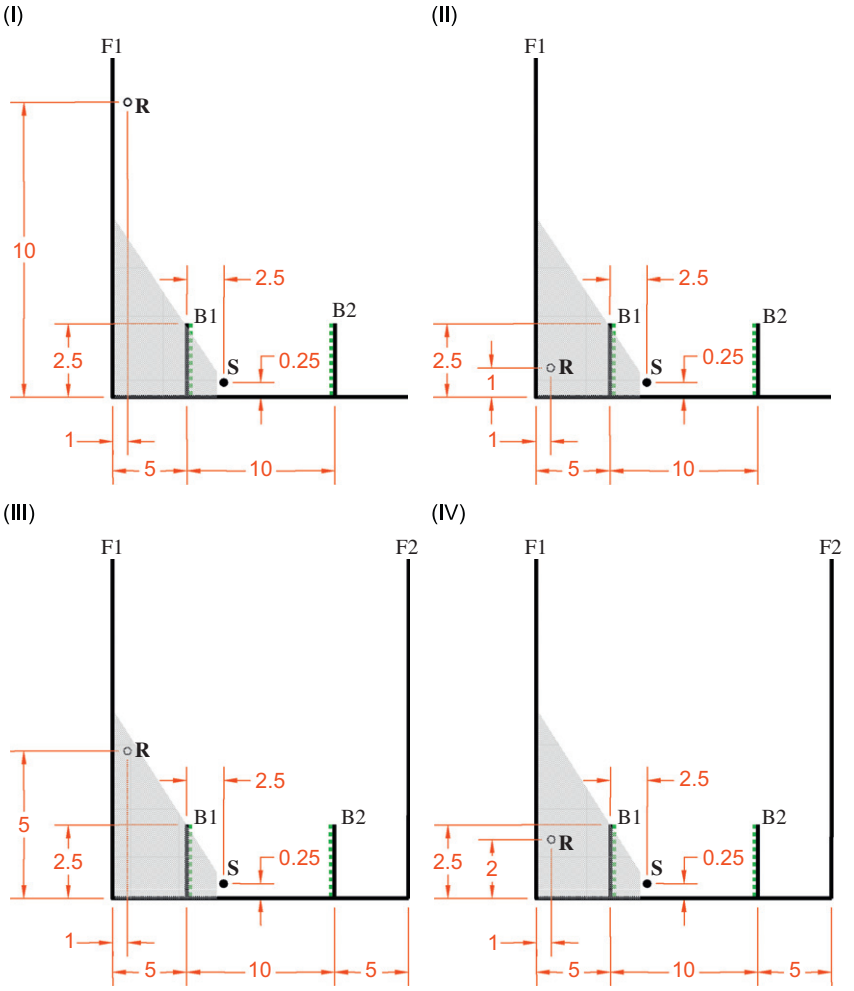

Fig. 3. Configurations used for the numerical comparisons based on the image source method (ISM) and the boundary element method (BEM). The receivers are located at (I) $\Re = (1, 0, 10)$, (II) $\Re = (1, 0, 1)$, (III) $\Re = (1, 0, 5)$ and (IV) $\Re = (1, 0, 2)$. Cases (I) and (II) represent situations of parallel noise barriers placed in front of a building façade. Cases (III) and (IV) represent situations of parallel noise barriers placed in a street canyon. In all cases, the parallel noise barriers have absorptive inner surfaces. The impedance of these inner surfaces is calculated by the Delany and Bazley model with an effective flow resistivity of $40\,\mathrm{kPa\,s\,m^{-2}}$.

they are usually the case in most practical urban situations. It is straightforward to study the effect of porous pavements and absorptive façades in the ray model. However, we shall not pursue along this direction in the current paper. It will be a subject of future publications.

The inner surfaces of the parallel barriers are characterized acoustically by a specific normalized impedance, Z. Its value is computed by the Delany and Bazley model as follows:

$$Z = 1 + 0.0511 \times \left(\frac{\sigma_e}{f}\right)^{0.75} + \mathrm{i}0.0768 \times \left(\frac{\sigma_e}{f}\right)^{0.73}, \tag{24}$$

where f is the frequency in Hz and σ_e the effective flow resistivity in $\mathrm{Pa\,s\,m^{-2}}$. Unless stated otherwise, the effective flow resistivity is chosen to be $40\,\mathrm{kPa\,s\,m^{-2}}$ in our numerical simulations.

In the present study, the height of the building façade is taken as 30 m, which should be sufficiently tall to ensure that any contributions due to the diffraction of the sound at the top edge of the façade are negligibly small. In the BEM formulation, we choose at least 10 elements per wavelength in order to ensure a higher

accuracy for the purpose of validation. The size of elements used in the current BEM computations for different frequencies are summarized in Table 1 for information.

We remark that a FORTRAN program for the BEM formulation was used to compute the sound fields for the two urban scenarios described earlier. A suite of MATLAB programs for the ray model was developed to compute the corresponding sound fields. In a preliminary study of the ray model computations, we find that variations in the sound pressure level generally become stable after about 60 reflections for the source frequency varying from 100 to 10,000 Hz. As a result, we simply set the maximum orders of reflections to be no more than 100 for both sides of the barriers at all receiver locations. This will lead to a simpler program with an acceptable numerical accuracy at the expense of a modest increase in the overall computational time.

In presenting the simulation results, the IL spectra are shown where it is defined as the reduction in sound pressure levels in the absence of the parallel barriers in an otherwise identical urban environment, i.e.,

$$\mathrm{IL} = 20\log_{10}\left(\frac{P_w}{P_{w/o}}\right) \tag{25}$$

with P_w and $P_{w/o}$ is the predicted sound fields with and without the presence of the barriers.

Fig. 4 shows the predicted IL spectra for cases (I)–(IV), see Fig. 3 for the geometrical configurations of these four cases. Although there are noticeable discrepancies for the predicted magnitudes at some frequencies between these two methods, the general trends of the IL spectra such as the places of the peaks and dips predicted by the ISM match well with those predicted by the BEM formulation. The levels of fluctuation in IL spectra reflect the phenomenon of interference of all contributory rays. The ISM is capable of predicting this wave interference effect. It is because the total sound field is computed by summing the contributions coherently from a finite number of image sources produced by multiple reflections of the boundary surfaces. In order to have a better quantitative comparison, the predicted results have also been compared in 1/3 octave bands for a range of center frequencies varying from 200 to 4000 Hz as shown in the inset figure. These octave band analyses have been widely used for studying the impact of the transportation noise.

Compared with the narrowband spectrum, the large fluctuations in the IL are averaged out in the plots and the inset figure also showed good agreements in terms of constructive and destructive interferences over the 1/3 octave bands. These plots highlight the importance for including the information of the magnitude and phase of each ray in the prediction model. The traditional energy-based ray model cannot be used to predict this wave phenomenon.

In Fig. 4(b)–(d), we show the predicted results for the receivers situated in the shadow zone at various heights above the ground. The results predicted by the two methods show that IL varies from 5 to 20 dB for the one-third the octave bands with center frequencies ranging from 200 to 4000 Hz. The predicted IL increases with increasing frequency. For a receiver located in the illumination zone (see Fig. 4(a)), the predicted IL varies from −3 to 4 dB in the spectrum.

For the predicted sound fields in the shadow zone, the agreement between the two numerical models is not as good as the results shown in the illumination zone. However, the ISM predicts fairly accurately the position of the 'peaks' and 'dips' in the narrow-band frequency spectrum although there are some noticeable discrepancies in the predicted magnitudes between the results of BEM and the ray model. It is worth noting that the predicted results according to the ISM generally tend to have higher fluctuations than the predictions based on the BEM formulation. It is because the ISM sums a large number of small terms with different

Table 1
The element size used for the implementation of the boundary element method

Frequency/Hz	Number of elements per wavelength
<500	100
501–800	40
801–1000	20
>1000	10

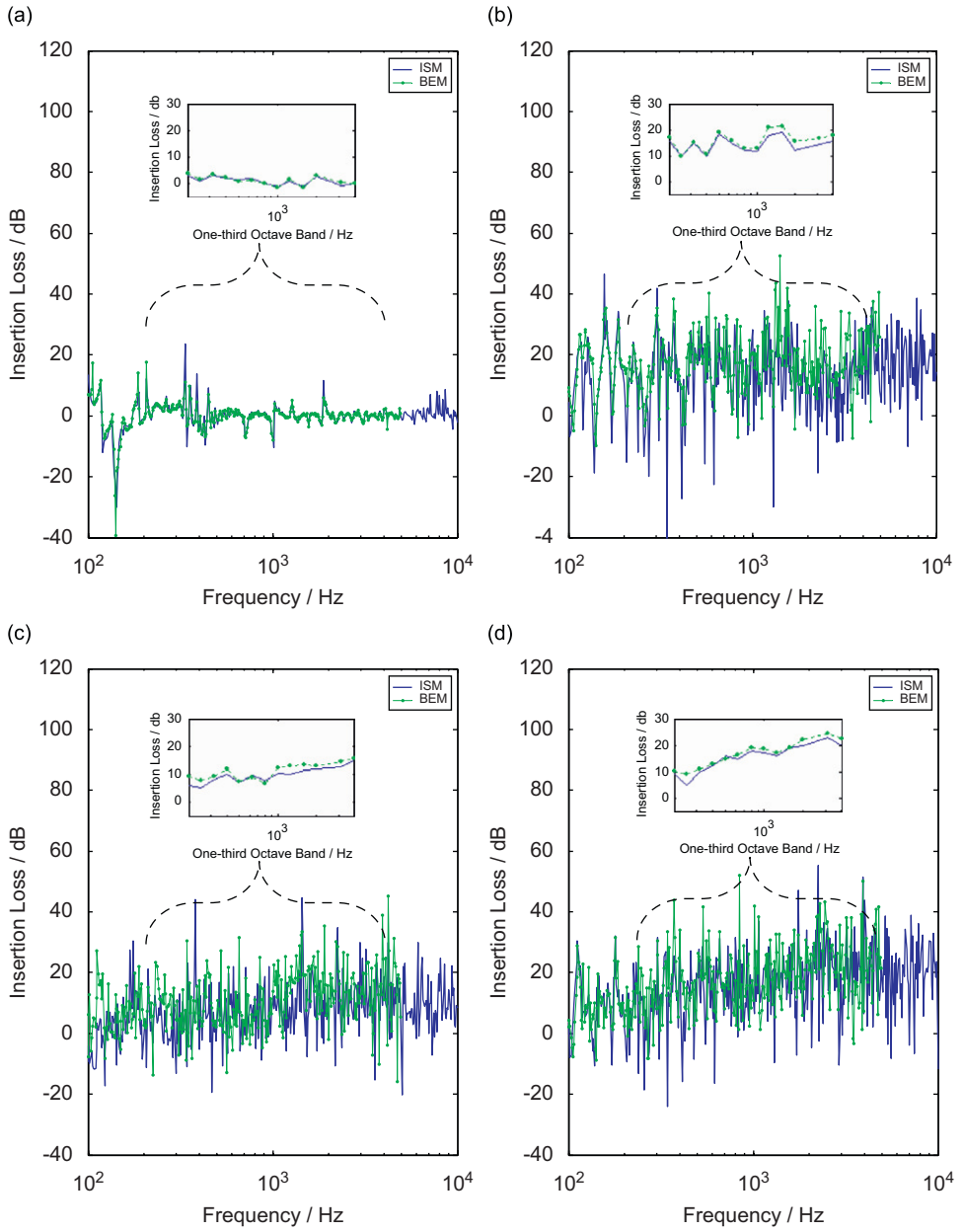

Fig. 4. The spectrum of insertion losses for (a) case I, (b) case II, (c) case III and (d) case IV for Fig. 3. The solid line represents predictions by the image source method (ISM), and the dashed line with dots represents numerical predictions based on the boundary element method (BEM). Inset figures: Comparisons of the predicted insertion loss between ISM and BEM with one-third octave band frequencies varying from 200 to 4000 Hz.

phases. This can lead to a higher fluctuation in the predicted sound fields, especially, at high frequencies due to the truncation errors of the ray series.

We note here that the predicted results agree to within 0.3 dB between the two numerical schemes for the case of a single façade with the receiver at the illumination zone, see Fig. 4a. For the receiver in the shadow zone (Fig. 4c–d), the image source model consistently under-predicts the IL for all 1/3 octave bands when the results are compared with that of the BEM predictions. Nevertheless, the results from the two prediction schemes are generally in reasonably good agreement with an average difference of about 1 dB.

The IL spectrum is dependent on the geometrical configurations of the problem such as the relative locations of barriers, façades, source and receiver. Similar results can be obtained when the geometrical configurations are changed and some of these numerical results are shown elsewhere [13]. The BEM formulation requires substantially higher computational resources especially at high frequencies than the ISM.

A FORTRAN program was used to compute the sound field for a pair of absorbent parallel noise barriers locating in a street canyon with a source operating at 5 kHz. These are the highest frequencies we computed in the numerical simulations using the BEM formulation. The computational time for the BEM formulation will increase exponentially for the source frequency extending beyond 5 kHz and for the façade surfaces higher than 25 m.

On the other hand, we have developed a MATLAB program for the image source model, which was used to predict the sound fields for the present study. The computational time is generally independent of the source frequencies for the image source model. Using the same desktop computer, the computational time was significantly reduced for a source frequency operating at 5 kHz. It is straightforward to develop a FORTRAN program that can be used to reduce the computational time further. However, the MATLAB program is considered adequate for the present study.

4. Experimental validation of the image source model

A model (with a scale of one-tenth) was built which was placed either in front of a model façade or in a model street canyon for the present experimental study. Measured data were obtained in an anechoic chamber of size 6 m × 6 m × 4 m (high) for validating the image source model. The experimental set-up for the parallel barriers in a street canyon is shown in Fig. 5, which has a comparable source/receiver configuration discussed in the last section. The set-up for the parallel barriers in front of a façade is achieved by removing the wooden board at the far right as shown in Fig. 5. The façade and ground surfaces are made of 8.5 mm thick wooden boards, which were varnished to prevent sound leakage. Prior measurements [13] were conducted to measure the acoustic characteristic of the varnished wooden boards. We found that they can generally be treated as a perfectly reflecting surface.

The pair of noise barriers was constructed with 3-mm-thick aluminum plates of 4.5 m long and with a height of 0.5 m. The pair of noise barriers was placed parallel to each other at a distance of 0.75 and 1.5 m in front of the near-side façade. The height of each façade surface was 2.44 m, which was sufficiently high to minimize the possible contribution of the diffracted sound fields at the top edge. A layer of fibreglass of 25 mm thick and

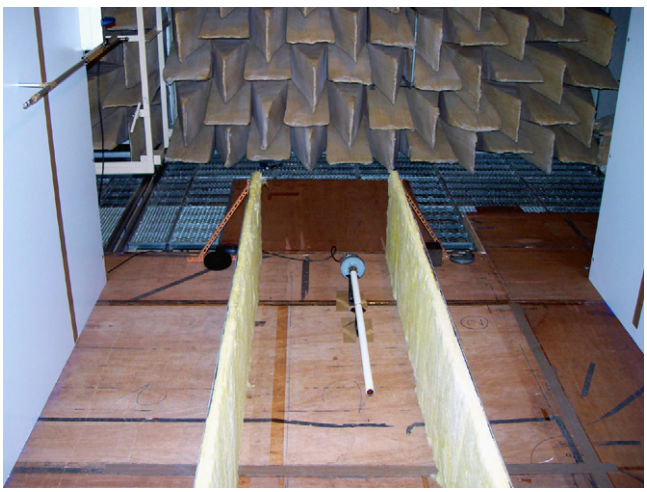

Fig. 5. The experimental set-up for indoor measurements showing a pair of absorbent parallel barriers placed in a street canyon.

density of 48 kg m^{-3} was attached on the surfaces of the parallel noise barriers facing each other. A hard back layer model was used to model the characteristic impedance, Z', of the barrier surface:

$$Z' = Z \coth(-ikd), \tag{26}$$

where k and d are, respectively, the propagation constant and the layer thickness of the fibreglass. The characteristic impedance Z of the fibreglass is calculated by the Delany and Baxley model given in Eq. (24). Prior indoor measurements [13] were conducted to characterize the acoustic properties of the fibreglass used in the current study. Using Eq. (24), we found that the acoustic impedance can be estimated with an effective flow resistivity of 72.4 kPa s m^{-2} with a layer thickness of 25 mm.

The primary objective of our indoor measurements is to provide useful experimental data for the validation of our numerical models. They are not designed as a proper scale-model experiment for urban environments as was conducted by others [17]. Hence, no attempt was made to select the most appropriate materials to model those absorption materials used in outdoor situations. Rather, we choose a hardwood board to model a hard ground, surfaces covered with fibreglass to model a pair of parallel absorbent barriers. Comparisons of the indoor experimental results and theoretical predictions should shed light on the validity of the ray model developed in the current study.

We conducted a series of indoor experiments using a Tannoy speaker mounted on a long brass pipe with length of 1.5 m and diameter of 25 mm. It is used to simulate an omni-directional point source. The measured results for the directional characteristic of the point source from preliminary test suggests that the deviation in the directivity pattern for all directions is within 1 dB for all frequencies above 250 Hz.

In all measurements, the point source was located 0.5 m from the left barrier and at a height of 0.125 m above the ground. A B&K 4942 microphone, which was connected to a B&K 2671 preamplifier and a B&K NEXUS conditional amplifier, was used as the receiver. The microphone was placed at 0.123 m in front of the vertical wooden boards at various heights. A special type of test signals called maximum-length sequence (MLS) was employed to obtain the experimental data. The MLS signals were generated by the MLSSA 2000 card [18], transferred via the built-in DA-converter, and boosted by a B&K 2713 power amplifier. The deterministic nature of the MLS provides an excellent signal-to-noise ratio, which is ideal for the current indoor measurements. The IL spectra used for comparison were obtained by measuring the respective transfer function with and without the noise barriers.

A selected set of experimental configurations, which is illustrated in Figs. 6 and 8, is used for studying the sound fields in two urban scenarios: (a) when a pair of parallel barriers is flanked by a row of tall buildings, and (b) when the parallel barriers are placed in a street canyon. The receivers are chosen at 0.123 m away from the near-side façade F1 and with heights of (I) 0.1 m, (II) 0.3 m, (III) 0.5 m and (IV) 1.5 m above the ground. For the selected source/receiver geometries, the receiver was situated at the shadow zone for cases (I), (II) and (III). The receiver was located at the illumination zone at case (IV).

We show IL spectra with frequencies varying from 100 to 10,000 Hz in the following plots although valid experimental data are not generally expected for frequencies below 500 Hz because of the size of the anechoic chamber and the size of the scaled model used in the measurements.

Fig. 6 shows the corresponding source/receiver geometry used in experimental measurements and numerical simulations for the absorbent parallel barrier placed in front of a façade surface. The measured and predicted IL spectra for cases (I)–(IV) are shown in Fig. 7. For the narrow-band spectra, predicted and measured results show significant fluctuations in the IL spectra. These results reflect the phenomenon of complex wave interference due to the contributions from different image sources that have comparable magnitudes but with different phases. There is a general trend of the IL spectra with a pattern of constructive and destructive interferences as observed in the experimental data. These interference patterns are predicted reasonably well by the ISM and the BEM formulation. For the plots of the 1/3 octave bands as shown in the inset of Fig. 7, the image source model agrees well the trend predicted by the BEM formulation. The image source model and BEM predictions are generally in accord with experimental measurements. Compared with the narrow-band spectrum, the large fluctuations in the IL are 'smoothed' out in the plots of the one-third octave spectra.

Next, we show a comparison of the experimental results with the theoretical predictions for the case of the parallel barrier placed in a street canyon, see Fig. 8 for the respective geometrical configurations for

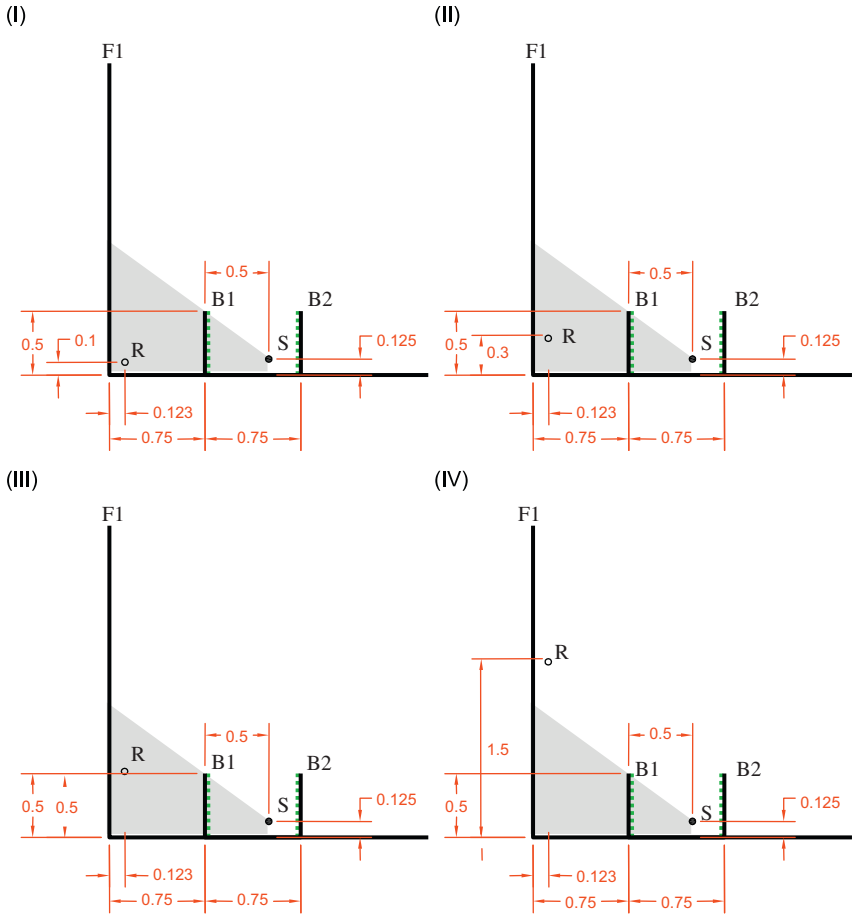

Fig. 6. Configurations used for the theoretical and experimental comparisons. The receivers are located at (I) $\Re = (0.123, 0, 0.1)$, (II) $\Re = (0.123, 0, 0.3)$, (III) $\Re = (0.123, 0, 0.5)$ and (IV) $\Re = (0.123, 0, 1.5)$ with parallel barriers placed in front of a building façade. In all cases, the parallel barriers have absorptive inner surfaces of 0.025 m thick. The impedance of these inner surfaces is calculated by the Delany and Bazley model and the thin-layer model with an effective flow resistivity of 72.4 kPa s m^{-2}.

cases (I)–(IV). In Fig. 9, we display the comparisons of the experimental results with the numerical predictions according to the ISM and the BEM formulation. There is a notable increase in the number of image sources in this urban scenario. Because of the presence of an additional building façade at the far side, the measured and predicted IL spectra show more fluctuations (cf. Figs. 7 and 9) due to the increase in interference of additional image sources. It becomes even more obvious for case (IV) when the receiver is located in the illumination region. Good agreements in terms of the fluctuation patterns are also demonstrated in Fig. 9 for the four selected receiver positions. Again, as shown in the inset figure, these large fluctuations in the sound fields are smoothed out in the 1/3 octave bands IL spectra. The image source model and BEM predictions both show tolerably good agreement with experimental measurements.

5. Case study

To illustrate the acoustic performance of absorbent parallel barriers when they are erected in a complex urban environment, this section is devoted to the numerical simulations for a typical highway of 40 m wide. The geometrical configuration of this problem is similar to that described in Section 3. The street canyon is modelled by two parallel flat façade surfaces perpendicular to the ground. The pair of noise barriers is 5 m

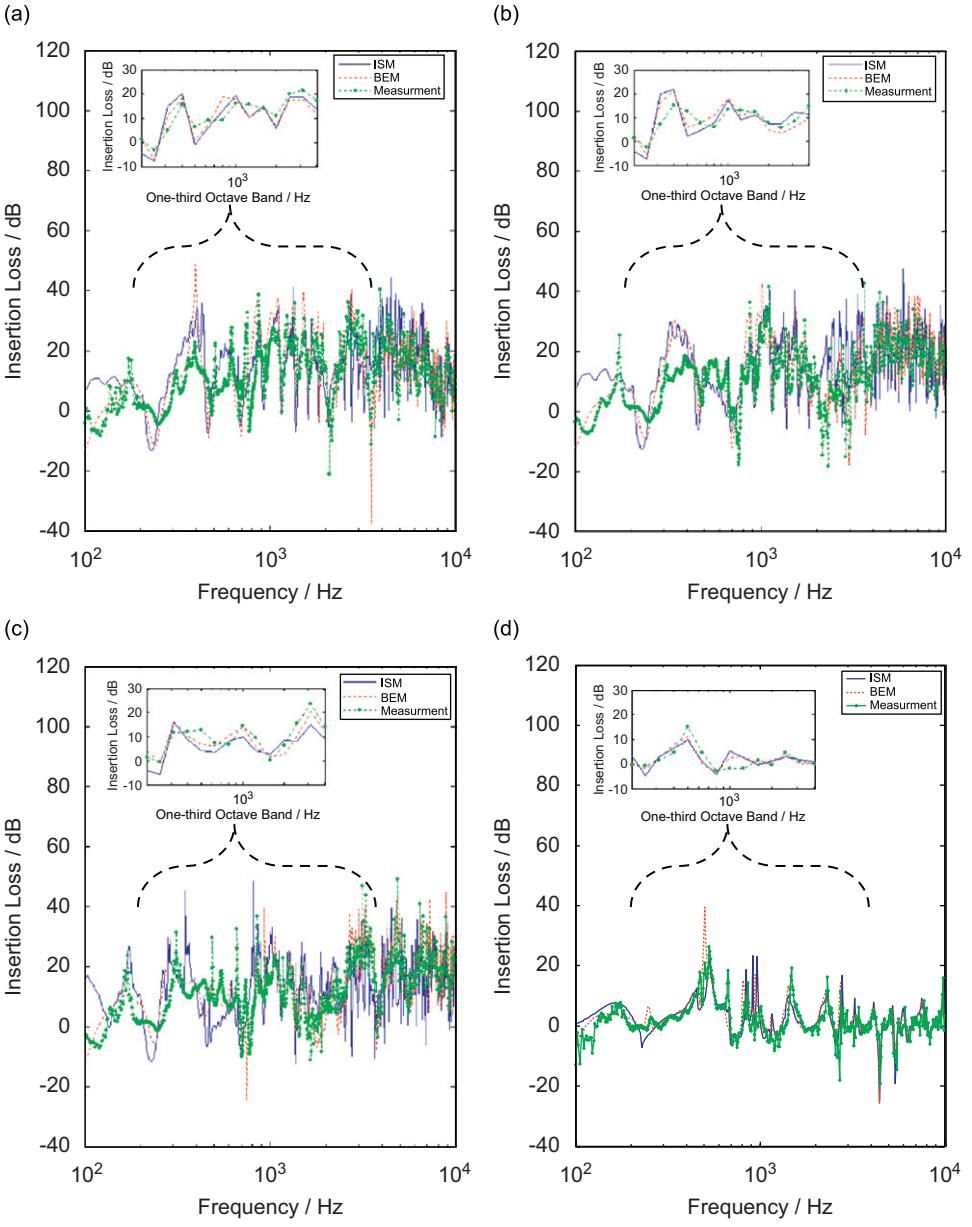

Fig. 7. The spectrum of insertion losses for (a) case I, (b) case II, (c) case III and (d) case IV for Fig. 6. The solid line represents predictions by the image source method (ISM), the dashed line represents numerical predictions based on the boundary element method (BEM), and the dashed line with dots represents results from experimental measurement. Inset figures: comparisons of the insertion loss between measured and predicted results in one-third octave band frequencies varying from 200 to 4000 Hz.

high and the separation between them is 20 m. The near side is situated at a distance of 10 m from the left building façade and the far-side barrier is located at a distance of 10 m from the right building façade. Vehicles are represented by a point source located at 6 m from the near-side barrier. The impedance of the barrier surfaces facing each other is calculated by using Eqs. (24) and (26) for a layer of porous materials on a hard-back. The assumed effective flow resistivity σ_e and thickness of material d, respectively, in Eqs. (24) and (26) are 50 kPa s m^{-2} and 10 cm.

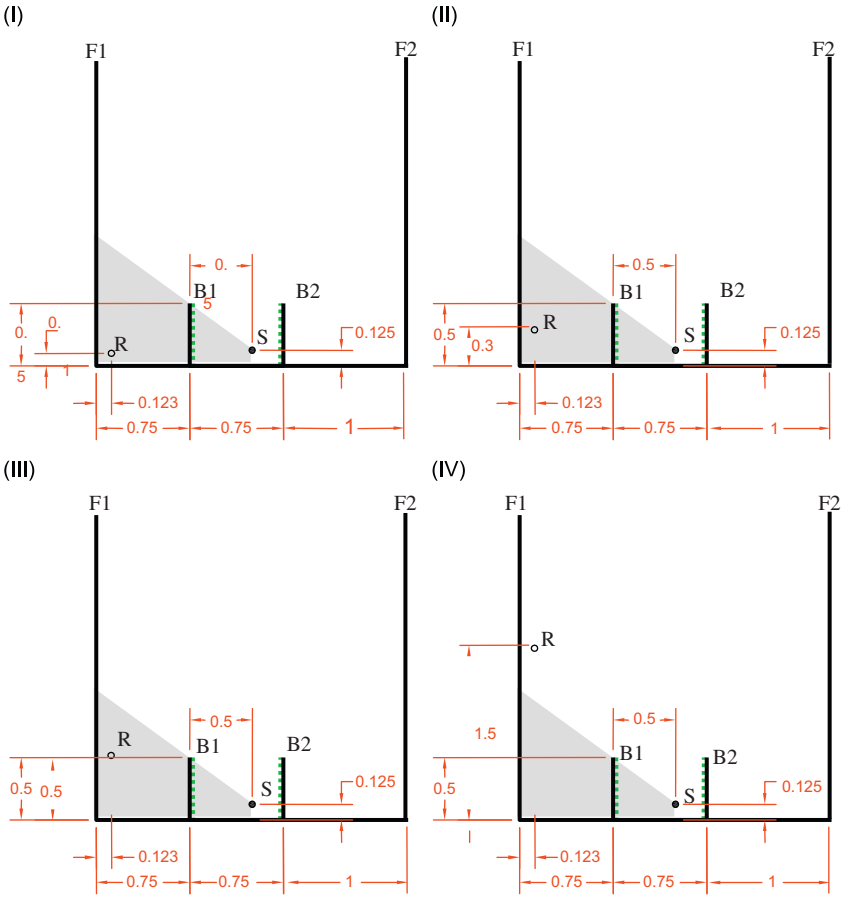

Fig. 8. Same as Fig. 6 except that an extra facade surface is located at 2.5 m away from the left-side façade representing the case of a street canyon.

Fig. 10 shows the IL obtained at the receivers located at (a) 1 m, (b) 5 m, (c) 10 m, (d) 15 m and (e) 20 m. As expected, the IL fluctuations as can be seen in the narrow-band plots are due to the wave interferences caused by multiple reflections. When the receiver is located deeper in the shadow zones, more fluctuations in the narrow-band spectra can be observed. The comparison of IL spectra in one-third octave bands is shown in the right column of Fig. 10. When the receiver is placed in the shadow zone as in Fig. 10(a)–(c), the IL is generally higher for the absorbent parallel noise barriers than the hard parallel noise barriers, i.e., an improvement of the shielding efficiency. However, the improvement becomes insignificant when the receiver is located at the illumination zone, see Fig. 10(d) and (e).

6. Conclusion

The evaluation the acoustic performance of absorbent parallel barriers placed in front of building façade and in a street canyon is presented in this paper. The suitability of using a ray model to predict the sound fields in a complex urban environment is also explored. The ray model is based on the ISM using the classical theories of geometrical acoustics and outdoor sound propagation. It has been demonstrated that the ray model agrees well with the other more accurate wave-based numerical approach in predicting the sound fields in these complex environments. In addition, the ray model has also proved to be sufficiently accurate that the numerical results are in tolerably agreements with indoor experimental data.

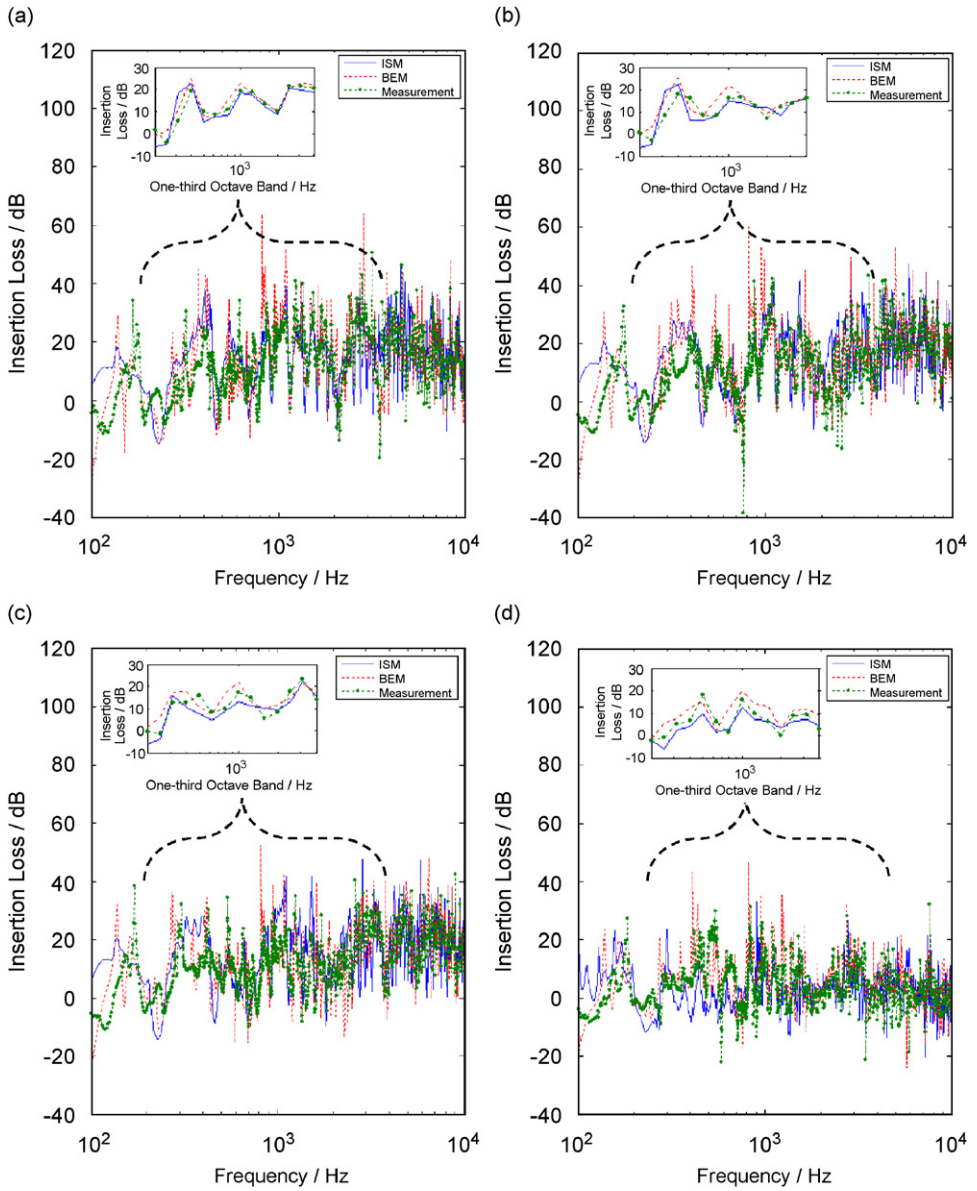

Fig. 9. The spectrum of insertion losses for (a) case I, (b) case II, (c) case III and (d) case IV for Fig. 8. The solid line represents predictions by the image source method (ISM), the dashed line represents numerical predictions based on the boundary element method (BEM), and the dashed line with dots represents results from experimental measurement. Inset figures: Comparisons of the insertion loss between measured and predicted results in one-third octave band frequencies varying from 200 to 4000 Hz.

The ray model has a significant advantage of reducing the computational resources in which a desktop computer may be used to simulate the acoustic environments of a realistic urban scenario. In conclusion, the developed ray model is a valuable tool for the evaluation in the design stage due to its accurate prediction capability and high computational efficiency.

We show in a case study that the addition of sound absorption materials at the inner surface of barrier surfaces can lead to an improvement of the IL of the parallel noise barriers for those receivers located in the shadow zone. However, this improvement is insignificant if the receiver is located above penumbra region in the illumination zone.

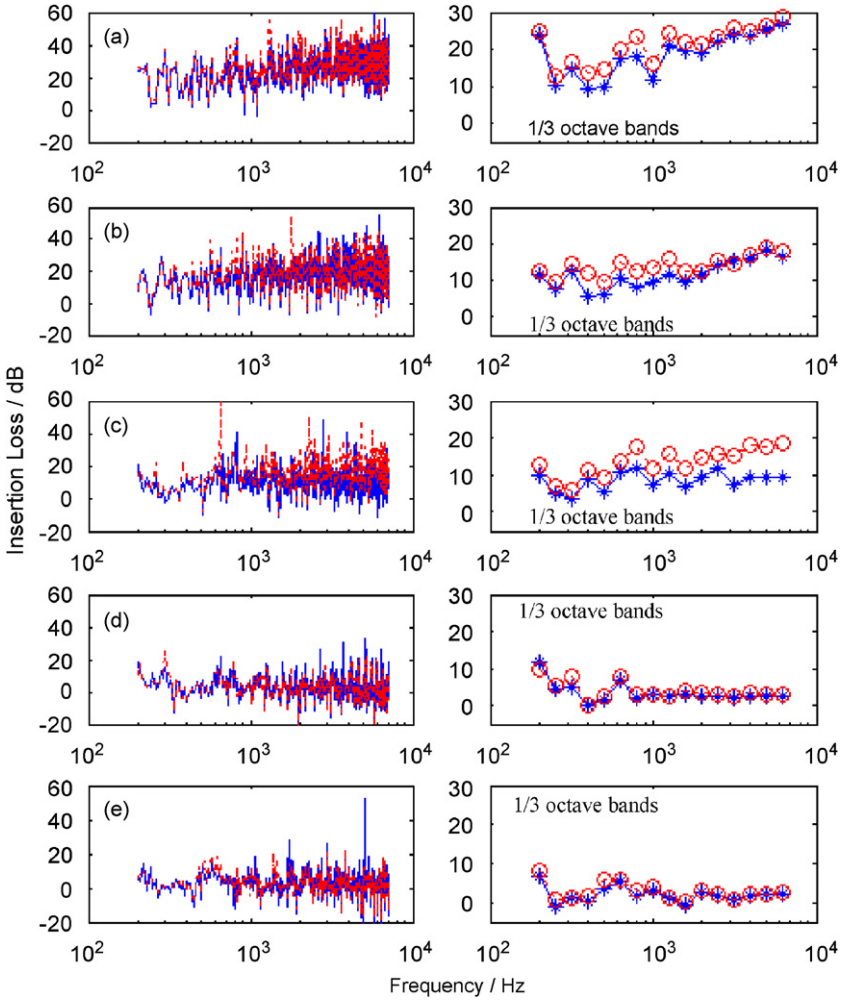

Fig. 10. The IL spectra of narrow bands (left column) and one-third octave bands (right column) for a highway of 40 m wide with two parallel absorbent barriers of identical height of 5 m. The receivers are located at (a) 1 m, (b) 5 m, (c) 10 m, (d) 15 m and (e) 20 m above the ground and 1 m in from of the left building façade. The impedance of the inner barriers surfaces is calculated by the Delany and Bazley model with a thin layer (effective flow resistivity of 50 kPa s m^{-2} and a layer thickness of 10 cm are used). The solid line represents parallel hard barriers predictions by the image source method (ISM), the dashed line represents parallel absorbent barriers predictions by the image source method (ISM).

Acknowledgements

This work was conducted while MKL was a visiting scholar at Purdue University and MPK was graduate student at the Hong Kong Polytechnic University. The research described in this paper was financed jointly by the Innovation and Technology Commission of the Hong Kong Special Administrative Region and the Mass Transition Railway Corporation Limited, through the award of an Innovation and Technology Fund under the category of the University-Industry Collaboration Programme (Project no. UIM/39). The authors gratefully acknowledge the Research Committee of the Hong Kong Polytechnic University for the facilities and technical supports provided throughout the period of the research. The authors thank Dr. Glenn H. Frommer of MTR Corporation for his encouragements and many useful discussions.

References

[1] D.A. Hutchins, D. Pitcarn, A laser study of multiple reflections within parallel barriers, *Journal of the Acoustical Society of America* 73 (1983) 2216–2218.

[2] C.J. Hurst, Sound transmission between absorbing parallel planes, *Journal of the Acoustical Society of America* 67 (1980) 206–213.

[3] D.A. Hutchins, H.W. Jones, Parallel barriers in the presence of ground surfaces, *Noise Control Engineering Journal* 23 (1984) 105.

[4] D.A. Hutchins, H.W. Jones, B. Paterson, L.T. Russell, Studies of parallel performance by acoustical modeling, *Journal of the Acoustical Society of America* 77 (1985) 536–546.

[5] S.N. Chandler-Wilde, D.C. Hothersall, Sound propagation above an inhomogeneous impedance plane, *Journal of Sound and Vibration* 98 (1985) 475–491.

[6] D.C. Hothersall, S.N. Chandler-Wilde, M.N. Hajmirzae, Efficiency of single noise barriers, *Journal of Sound and Vibration* 146 (1991) 303–322.

[7] D.C. Hothersall, D.H. Crombie, S.N. Chandler-Wilde, The performance of T-profile and associated noise barriers, *Applied Acoustics* 32 (1991) 269–287.

[8] P.A. Morgan, D.C. Hothersall, S.N. Chandler-Wilde, Influence of shape and absorbing surface—a numerical study of railway noise barriers, *Journal of Sound and Vibration* 217 (1998) 405–417.

[9] R. Panneton, A. L'Espérance, G.A. Daigle, Development and validation of a model predicting the performance of hard or absorbent parallel noise barriers, *Journal of the Acoustical Society of Japan (E)* 14 (1993) 251–258.

[10] W.J. Hadden, A.D. Pierce, Diffraction of sound around corners and over wide barriers, *Journal of the Acoustical Society of America* 69 (1981) 1266–1276.

[11] Y. Miki, Acoustical properties of porous materials—modification of Delany–Bazley models, *Journal of the Acoustical Society of Japan* 11 (1990) 19–24.

[12] K.M. Li, S.H. Tang, The predicted barrier effects in the proximity of tall buildings, *Journal of the Acoustical Society of America* 114 (2003) 821–832.

[13] K.M. Li, M.P. Kwok, M.K. Law, A ray model for hard parallel noise barriers in high-rise cities, *Journal of the Acoustical Society of America* 123 (2007) 121–132 (see also M.P. Kwok, Noise Barriers in a Complex Urban Environment, M. Phil. Thesis, Department of Mechanical Engineering, The Hong Kong Polytechnic University, 2006).

[14] T.F.W. Embleton, Tutorial on sound propagation outdoors, *Journal of the Acoustical Society of America* 100 (1996) 31–48.

[15] K.M. Li, K.K. Iu, Propagation of sound in long enclosures, *Journal of the Acoustical Society of America* 116 (2004) 2759–2770.

[16] P. Koers, Diffraction by an absorbing barrier or by an impedance transition, *Proceedings of Internoise* 83 (1983) 311–314.

[17] K.V. Horoshenkov, D.C. Hothersall, S.E. Mercy, Scale modelling of sound propagation in a city street canyon, *Journal of Sound and Vibration* 223 (1999) 795–819.

[18] D.D. Rife, *Maximum-Length Sequence System Analyzer, Reference Manual, Version 10W*, 1987–1988.